

Review

# A Review on the Optimal Design of Magnetic Nanoparticle-Based $T_2$ MRI Contrast Agents

Nina Kostevšek 

Department for Nanostructured Materials, Jožef Stefan Institute, 1000 Ljubljana, Slovenia; nina.kostevsek@ijs.si

Received: 12 February 2020; Accepted: 25 February 2020; Published: 28 February 2020



**Abstract:** Relaxivity  $r_2$  and thus the contrast efficacy of superparamagnetic nanoparticles (NPs) can be enhanced via either NP's magnetic properties or coating optimization. Numerous reports can be found about the investigation of the optimal iron oxide nanoparticles (IO NPs) size, shape, crystallinity and composition that yield high saturation magnetization ( $m_s$ ) values and, consequently, high  $r_2$  values. Although the use of an appropriate coating can boost up the NPs MRI contrast agent efficiency, this topic has been largely understudied. Therefore, in this review, the factors affording  $r_2$  enhancement of spherical magnetic NPs are discussed. Based on the literature, the requirements for an optimal surface coating that may increase  $r_2$  values and ensure stability and biocompatibility of NPs are listed. One of the best candidates that fulfil these requirements are liposomes with embedded magnetic NPs, so-called magneto-liposomes. The analysis of the literature elucidated the most appropriate phospholipid compositions for the relaxivity enhancement and for magneto-liposomes in vivo stability. Finally, the future directions in the development of NP-based contrast agents are given. For example, most of the synthetic NPs are recognized and eliminated as a foreign substance by the immune system. To overcome this issue, a design of a biomimetic, cell-membrane-based nanocarrier for contrast agents is proposed. Disguised with cell membranes, NPs or other active components can act as autogenous cells and thus ensure the inherent biocompatibility.

**Keywords:** nanoparticles; magnetic resonance imaging; liposomes; biomimetics

## 1. Introduction

Magnetic resonance imaging (MRI) has good anatomic resolution and excellent soft-tissue contrast imaging capabilities. Without using contrast agents, differences between diseased and normal tissues can be difficult to observe with MRI [1]. In clinics, the most commonly used longitudinal  $T_1$  contrast agents are gadolinium (Gd) chelates [2], and the most commonly used transverse  $T_2$  contrast agents are iron oxide nanoparticles (IO NPs) [3]. Importantly, since IO NPs are not associated with a risk of nephrogenic sclerosis, they serve as safer contrast agents compared with gadolinium chelates [4]. Additionally, IO NPs can better characterize differences in the microvascular permeability of benign and malignant breast tumors and other soft-tissue tumors; benign tumors show no or minimal IO enhancement, whereas malignant tumors show marked IO enhancement [5]. Since the mid-1990s, several iron-based MRI contrast agents have been developed. Up to now, only five IO NPs have been clinically approved for MRI [6,7]. These products are Feridex<sup>®</sup> (dextran-coated  $\gamma$ -Fe<sub>2</sub>O<sub>3</sub> NPs), Resovist<sup>®</sup> (carbodextran-coated Fe<sub>3</sub>O<sub>4</sub> NPs), Combidex<sup>®</sup> (dextran-coated Fe<sub>3</sub>O<sub>4</sub> NPs), Gastromark<sup>®</sup> (siloxane-coated Fe<sub>3</sub>O<sub>4</sub> NPs), and Faraheme<sup>®</sup> (carboxyhydrate-coated Fe<sub>3</sub>O<sub>4</sub> NPs). However, the majority of the above-listed IO systems have been withdrawn from the market due to either safety concerns or lack of profits [7]. The highest relaxivity  $r_2$  value is shown by Resovist<sup>®</sup> (189 mM<sup>-1</sup> s<sup>-1</sup>), which is still on the market. Therefore, there is a clear need for novel IO NPs-based imaging agents with a high safety margin and superior MRI properties. The contrast ability of a contrast agent can be quantitatively characterized by its longitudinal relaxivity ( $r_1$ ) or transversal

relaxivity ( $r_2$ ). Relaxivity is defined as proportionality constants between the contrast-agent-induced increase of the corresponding relaxation rate and the MR contrast agent concentration. By definition, contrast agents of high relaxivities can provide an equivalent contrast effect at relatively low doses [1]. Relaxivity  $r_2$  of superparamagnetic NPs can be enhanced via either NP's magnetic properties or coating optimization. Both contributions will be discussed in the following sections.

Numerous reports can be found about the optimal IO NPs size, shape, crystallinity and composition that yield high saturation magnetization ( $m_s$ ) values and, consequently, high  $r_2$  values [8]. The proton relaxation mainly occurs at the interface between a magnetic NP and its surrounding aqueous environment; therefore, NP coatings importantly influence  $T_1$  and  $T_2$  relaxation processes [1,9]. Even though the use of an appropriate coating can boost up NPs performance, this topic has been largely understudied. Therefore, in this review, the importance of the selection of an optimal NPs coating for more efficient NP-based MRI contrast agents will be discussed. In addition to enhanced contrast agent efficacy, the selected coating should provide excellent stability and biocompatibility as well.

## 2. Optimization of the NPs' Magnetic Properties

Relaxivity  $r_2$  can be written as [10]:

$$r_2 = \frac{1}{T_2} = \frac{256 \pi^2 \gamma^2}{405} m_s^2 V \frac{r^2}{D \left(1 + \frac{L}{r}\right)}, \quad (1)$$

where  $\gamma$  represents the gyromagnetic ratio of protons,  $m_s$  is the saturation magnetization of an NP,  $V$  is the NP's volume fraction,  $r$  is the radius of the NP,  $D$  is the diffusion coefficient of water molecules and  $L$  is the thickness of the surface coating. From Equation (1), it can be seen that the shortening of  $T_2$  relaxation time is directly proportional to the square of  $m_s$ , which suggests that systems exhibiting large  $m_s$  would be of interest. NPs with high  $m_s$  values more efficiently induce field inhomogeneity, influence a greater volume of water (i.e., the secondary sphere) and have greater possibility of relaxing diffusing water molecules [1]. However, several contributions have to be taken into account when discussing the magnetic properties of magnetic NPs.

The magnetic anisotropy energy,  $E_a$ , is the energy needed to reverse the magnetization from one stable state to another [11]. This energy tends to keep the magnetization in a particular crystallographic orientation, which is called easy axis. The easy axis dictates which direction the magnetization will be pointing at in the absence of an external magnetic field [12]. Important contribution to the magnetic anisotropy energy is derived from the crystal structure of a material, e.g., cubic, tetragonal and hexagonal. This contribution is called magnetocrystalline anisotropy. In addition, shape anisotropy has an important contribution to the magnetic properties of nanostructures. Shape anisotropy originates from the nanostructure's demagnetizing field and depends on the shape of the nanostructure. In a nonspherical particle, the demagnetizing field ( $H_d$ ) strengths are not equal for all directions.  $H_d$  is smaller for the long axis and larger for the short axis and can therefore create one or more easy magnetization axes. The demagnetizing field can be expressed as  $H_d = \Delta N \cdot M_s$ , where  $\Delta N$  is the difference in demagnetizing factors for different axes. For spherical particles,  $\Delta N$  is 0; therefore, there is no shape anisotropy present. For example, it was shown that the variation in the magnetic properties between spherical-, cubic-, star- and rod-shaped FePt NPs arised from different shape anisotropies [13], which can importantly influence  $r_2$  values as well. Since the optimization of magnetic properties is not the main focus of this review paper, all the equations are valid for spherical NPs, and correction factors for shape anisotropy are not taken into account.

Furthermore, in the nanoregime, due to increased surface-to-volume ratios, surface anisotropy also becomes significant. Finite-size effects result from the quantum confinement of electrons [14]. Upon increasing a surface-to-volume ratio, a contribution of a surface to an overall magnetization becomes significant. Surface atoms experience different environments than those in the core of a

particle; therefore, several types of defects might exist on the surface such as atomic vacancies, changes in the atomic coordination, dangling bonds and lattice disorder [15]. These surface defects result in uncompensated disordered spins, which influence the magnetization of the surface. Spins at the surface of the NP undergo nonlinear coupling, forming a disordered shell around an ordered core. This phenomenon is called spin canting [12]. Because the surface contribution is significant, the anisotropy constant is not directly proportional to the particle's volume and differs from the bulk anisotropy constant ( $K_V$ ) values [15]. Therefore, the term effective anisotropy constant ( $K_{eff}$ ) was introduced for materials with reduced sizes [16] and can be described as:

$$K_{eff} = K_V + \frac{S}{V} K_S, \quad (2)$$

where  $K_V$  is the bulk anisotropy constant,  $K_S$  is the surface anisotropy and  $S/V$  is the particle's surface-to-volume ratio. Magnetic anisotropy is larger for NPs (by a factor of  $10^1$ – $10^2$ ) than for bulk materials due to the large contribution of surface anisotropy [14]. Therefore, the saturation magnetization ( $m_s$ ) of NPs is lower than the bulk value and is known to be proportional to the NPs' size, according to Equation (3):

$$m_s = M_s [(r-d)/r]^3, \quad (3)$$

where  $M_s$  is the saturation magnetization of the bulk,  $r$  is the radius of an NP, and  $d$  is the thickness of a disordered surface spin layer [17–19]. Application of surface-functionalization groups on NPs (surfactants), for the NP suspension stability and/or for their biocompatibility [18], can influence the thickness of the disordered surface spin layer. Therefore, coating can directly influence  $m_s$ . From Equation (3), it can be seen that by increasing the size of NPs the  $m_s$  value and, consequently,  $r_2$  value can be increased. However, we are limited by the superparamagnetic size limit, above which NPs become ferromagnetic that limits their use for medical applications. Theoretical studies indicate that there are three different NP size regimes: (i) the motional average regime (MAR), (ii) the static dephasing regime (SDR), and (iii) the echo-limiting regime (ELR). Relaxivity  $r_2$  increases in the MAR with NP size increments and then the NP size reaches a plateau (SDR). With any further size increment to enable the NP size to fall in the ELR,  $r_2$  decreases. Accordingly, the highest  $r_2$  is achieved for NPs in the SDR, but the size of NPs used for MRI usually falls into the MAR in order to limit their uncontrolled aggregation, induced by strong ferromagnetic dipolar interactions [20].

One of the options for improving NPs' effects on the  $T_2$  relaxation times is to produce controlled clusters of magnetic NPs with an increased  $m_s$  value to make the NP size fall in the SDR regime. For example, IO NPs (size: 7.4 nm) were combined into clusters (size: 163 nm) in block polymer micelles [21], where the increase in the loading of IO NPs in the micelles from 12% to 42% caused an increase in  $r_2$  from 90 to 229  $\text{mM}^{-1} \text{s}^{-1}$ . Additionally, the preparation of multicore NPs leads to  $r_2$  increase. For example, when IO NPs were prepared in a form of multicore nanostructures, the  $r_2$  value increased by a factor of 1.8 with respect to that of single-core NPs [22]. A similar trend was observed in the case of FePt NPs with single-core and multicore nanostructures [23]. This was attributed to the increase of  $m_s$  in the case of multicore NPs due to the exchange coupling within multicore nanostructures.

### 3. Influence of a Coating on Relaxivity

When engineering an appropriate NPs coating, interactions between water protons and a magnetic centre should be taken into account. A three-sphere model divides  $r_1$  and  $r_2$  relaxivities into three contributions [1]: (a) the inner sphere relaxivity ( $r^{IS}$ ), where hydrogen nuclei from water can directly bind to the magnetic metal centre; (b) the second sphere relaxivity ( $r^{SS}$ ), where the magnetic metal centre interacts with long-lived hydrogen nuclei (e.g., diffusing water molecules and exchangeable protons) that are not directly bound to the metal centre; and c) the outer sphere relaxivity ( $r^{OS}$ ) that

comes from the surrounding bulk water and is constant for a specific environment. Based on this model, the relaxivity can be expressed as Equation (4) [24]:

$$r_i = r_i^{IS} + r_i^{SS} + r_i^{OS} (i = 1, 2). \quad (4)$$

A three-sphere model for magnetic NPs is schematically shown in Figure 1. For  $T_2$  contrast agents, the inhomogeneity of a magnetic field created by a magnetic centre is responsible for the MRI contrast, and its influence is extended to the second sphere. Therefore,  $r^{SS}$  contributes most to the  $r_2$  value [1]. From this perspective, the more water molecules diffuse into the secondary sphere of NPs, the greater the possibility of relaxing these molecules. Thus, the use of coatings that may exclude water from the NPs vicinity, hinder water diffusion or extremely prolong the water residency can cause a reduction in  $r_2$ .

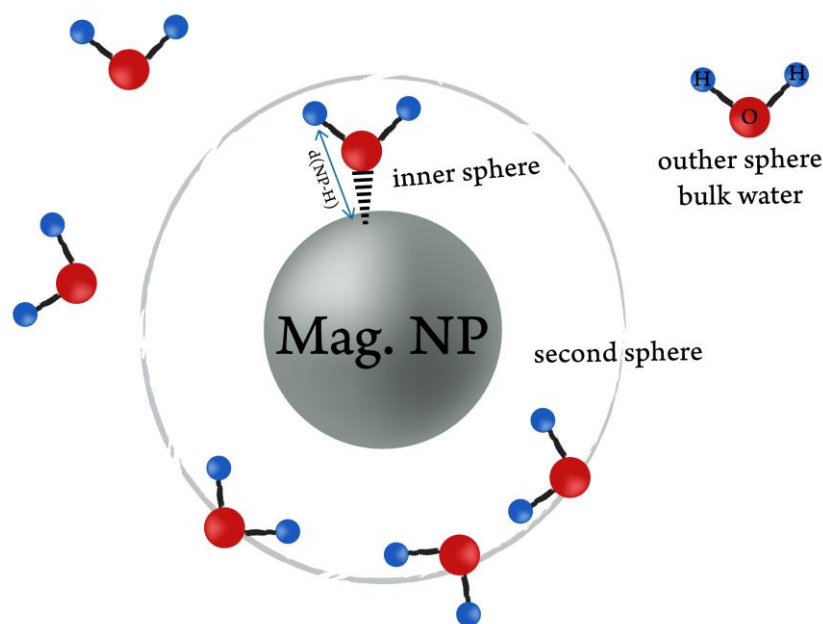


**Figure 1.** Schematic representation of a three-sphere model for a magnetic nanoparticle (NP).

Firstly, an increased distance between magnetic NPs and water molecules, e.g., thick coating, significantly decreases  $r_2$  values. This was demonstrated by an example of multicore FePt NPs, of which an initial  $r_2$  value of  $87 \text{ mM}^{-1} \text{ s}^{-1}$  decreased, upon coating with a 20 nm thick  $\text{SiO}_2$  coating [23] to  $53 \text{ mM}^{-1} \text{ s}^{-1}$  and further to  $47 \text{ mM}^{-1} \text{ s}^{-1}$  when an additional layer of Au was added [25]. TEM images and measured  $r_1$  and  $r_2$  values are shown in Figure 2. Hence, it can be seen that a thin coating is preferred to maintain high  $r_2$  values.

Secondly, coatings can have a direct influence on magnetization [1]. The capping ligands of NPs may affect the arrangement of surface atoms by reducing/increasing surface canting effects, thus increasing/decreasing magnetization. Thirdly, NP coatings may influence the magnetic field inhomogeneity spreading around NPs, which is a key parameter for  $r_2$  [26]. Ligands that are rich in  $\pi$ -electrons undergo circulation and create small local magnetic fields, thus increasing magnetic field inhomogeneity and  $r_2$  values. For example, double bonds in unsaturated phospholipids enhanced  $r_2$  values [1].

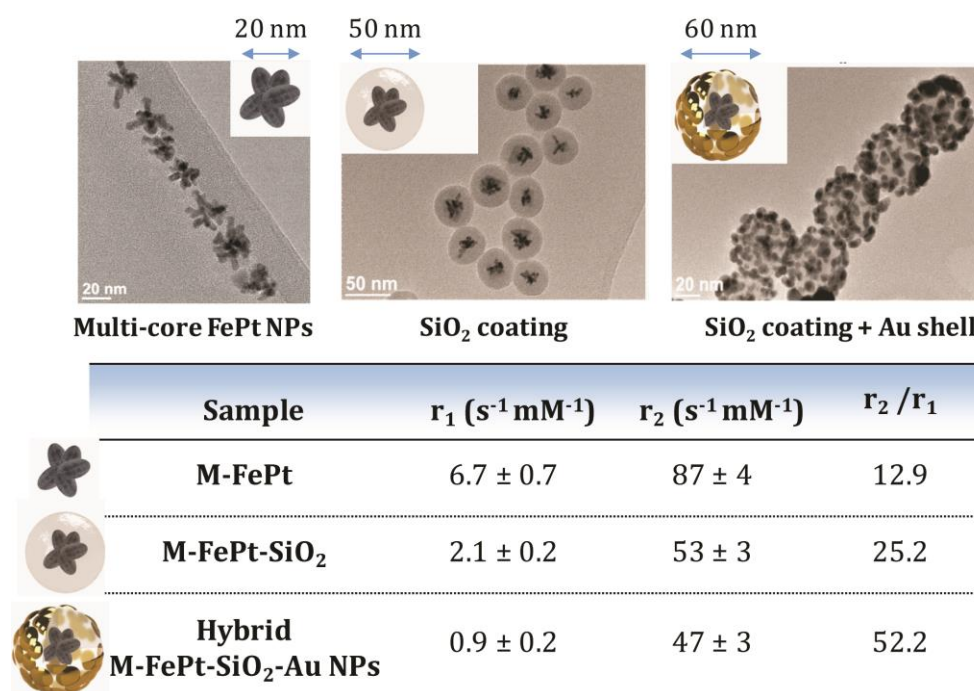


**Figure 2.** Influence of coating thickness on  $r_1$  and  $r_2$  relaxivity values. Adapted with permission from [23,25].

Finally, a critical factor for  $r_2$  is the diffusion dynamics of water molecules in the magnetic field gradients, i.e., the number of water molecules diffused into the secondary sphere of the contrast agent and their residency time within the region. Therefore, functional groups providing a highly hydrated surface are beneficial to amplify MR signals. For example, the phosphocholine head group had a high hydration number, where 25–30 water molecules were needed to completely hydrate the phosphocholine head group, in contrast to the ethanolamine head group hydration number (10–12 water molecules) [27]. Furthermore, not only hydration numbers but also water exchange rates are important. In other words, not only surface should be highly hydrated, but the relaxed water molecules should be quickly replaced by the bulk water molecules. In this way, a single particle can influence more water molecules and therefore lower concentrations of NPs are needed to achieve a stronger signal decrease and thus a better contrast of an image. For example, water exchange rates can differ by three orders of magnitude when comparing different functional groups (phosphonate and phenolate >  $\alpha$ -substituted acetate > acetate > hydroxamate and sulfonamide > amide, pyridyl and imidazole) [28]. This indicates that the phosphonate group on the surface should increase  $r_2$  relaxivity to a larger extent compared to other functional groups. In summary, the requirements for an optimal surface coating that may increase  $r_2$  values are shown as following:

1. Thin coating to minimize the distance between a magnetic core and water molecules;
2. Highly hydrated surface;
3. Fast water exchange rate;
4. Ligands containing  $\pi$ -electrons, which increase magnetic field inhomogeneity;
5. Biocompatibility of the coating and stability in biologically relevant media. Clinically approved moieties are prioritized due to an easier translation from a lab scale to a market scale.

One of the best candidates that fulfil the above-mentioned requirements are liposomes with embedded IO NPs, so-called magneto-liposomes. Liposomes are spherical vesicles consisting of a thin phospholipid bilayer. The phosphocholine head group ensures high hydration numbers and fast exchange rates. Phospholipids containing double bonds have more fluid bilayers and thus show a

faster water exchange rate compared to saturated counterparts, which significantly influences the  $r_2$  relaxivity. Importantly, liposomes are the most clinically approved nanosized delivery systems [29], which proves their biocompatibility. Furthermore, their structure allows for the encapsulation of additional active components in their aqueous cores, offering a great platform for the preparation of multifunctional NPs for theranostics. Therefore, a review of magneto-liposomes for MRI applications to elucidate the most appropriate phospholipid composition, and NPs location for relaxivity enhancement will be given in the next section.

#### 4. Magneto-Liposomes as $T_2$ Contrast Agents

Magneto-liposomes can have either hydrophobic NPs in a bilayer (Figure 3a) or hydrophilic magnetic NPs in a liposomal core (Figure 3b). A few reports have been published, using magneto-liposomes as MRI contrast agents [30–39]. Magneto-liposomes suspensions were tested for ex vitro [31–33,35,39] or in vivo imaging [30,34,36–38]. The majority of these studies reported the encapsulation of hydrophilic IO NPs in the liposomes' aqueous core, to reduce particles aggregation under physiological conditions, enhance tissue accumulation and improve their imaging capabilities. In contrast, only one study has been published with hydrophobic IO NPs embedded in the lipid bilayer of liposomes [39]. A detailed list of the above-mentioned references with a summary of their experimental conditions (sizes of IO NPs and their locations in liposomes, liposomal formulation, concentration range used for the determination of  $r_2$ , maximum  $r_2$  value and in vivo conditions) can be found in Table 1. Abbreviations for phospholipids are used in the paper. Their full chemical names are listed in Table 2.

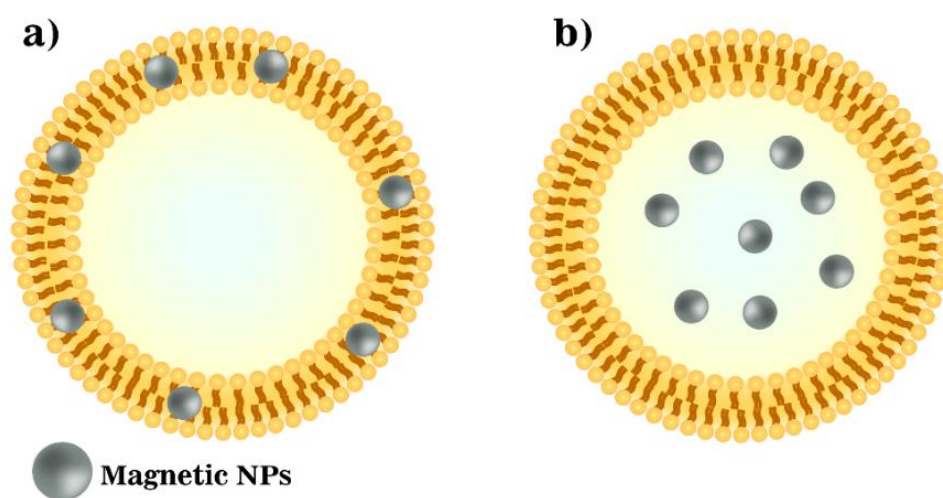


**Figure 3.** Schematic illustration of two types of magneto-liposomes: (a) hydrophobic NPs in a bilayer of magneto-liposomes; (b) hydrophilic magnetic NPs in the core of magneto-liposomes.

**Table 1.** List of all studies using magneto-liposomes for magnetic resonance imaging (MRI) applications with a summary of their experimental data (sizes of IO NPs and their locations in liposomes, liposomal formulation, concentration ranges used for the determination of  $r_2$ , maximum  $r_2$  values and in vivo conditions). Chol is abbreviation for cholesterol.

Reference (NPs Location)	Ex Vitro Suspension Only (Formulation, Fe Concentration Range and Maximum $r_2$ Value)	In vivo (Concentration Used and Administration Route)
[30] Shen et al., 14 nm IO NPs in the core	DPPC/Chol (80/20 mol%) 0–0.8 mM $r_2 = 20.49$	Intravenous injection of 200 $\mu$ L of MLs with a $\text{Fe}_3\text{O}_4$ concentration of 2 mg/mL + magnet next to the tumor. Tumor appeared 59% darker.
[31] Carvalho et al., 6 nm IO NPs core	Soybean PC + Chol 0–2.5 mM Max $r_2$ value = 143.69 without Chol	/
[32] Skouras et al., size not specified, in the core	Concentration range not specified, only relaxivities shown	/
[33] Garnier et al., 7 nm iron oxide (IO) NPs in the core	DOPC/Chol (75/25 mol%) 0–0.8 mM Maximum $r_2$ value = 323	/
[34] Marie et al., 13 nm IO NPs in the core	EPC/DSPE-polyethylene glycol (PEG) <sub>2000</sub> /Rho-PE = 94/5/1 0–0.2 mM Maximum $r_2$ value = 259	Intravenous injection of 200 $\mu$ L MLs (122.5 $\mu$ moles lipids and 533 $\mu$ moles IO per kg) + magnet next to the tumor. Tumor appeared darker
[35] Faria et al., 11 nm IO NPs in the core	SPC/Chol = 1/0.5 no conc. ranges Agar phantoms–T2 images slightly darker	/
[36] Martina et al., 17 nm IO NPs in the core	Egg-PC/DSPE-PEG <sub>2000</sub> (95/5) 0.02–10 mM Maximum $r_2$ value = 130	Intravenous of 200 $\mu$ L of MLs (20 mM total lipid and 25 mM Fe). Tumor was 22% brighter on $T_1$ image.
[37] Béalle et al., 7 nm IO NPs in the core	DPPC/DSPC (90/10) 0–1 mM max $r_2$ value = 267.9	DPPC/DSPC/Rhod-PE/DSPE-PEG (94/10/1/5) 100 $\mu$ L of MLs with 0.1 mM Fe retro-orbital venous sinus injection + magnet next to the tumor. Darker contrast observed in the tumor
[38] Guo et al., 4 nm IO NPs in the bilayer	DPPC/Chol/SA/DSPE-MPEG <sub>2000</sub> -MTX 0–1 mM $T_2$ -weighted images Maximum $r_2$ value = 60.06	Intravenous injection of 0.2 mL of 2 mg/kg (DOX equivalent dose) + tumor next to the tumor. Colored $T_2$ images
[39] Martínez-González et al., 5 nm hydrophobic IO NPs in the bilayer Hydrophilic NPs not in the liposomes, but forming branched–linear clusters	DMPC, DMPC/Chol, DMPC-PS, DOPC, DOPC/Chol, DOPC-PS 0–0.12 mM Maximum $r_2$ value = 995 for DOPC-PS	/

**Table 2.** List of phospholipids mentioned in the paper with their full chemical names.

Abbreviation	Chemical Name
DOPC	1,2-dioleoyl-sn-glycero-3-phosphatidylcholine
DPPC	1,2-dipalmitoyl-sn-glycero-3-phosphatidylcholine
DSPC	1,2-distearoyl-sn-glycero-3-phosphatidylcholine
DMPC	1,2-dimyristoyl-sn-glycero-3-phosphocholine
DSPE-PEG <sub>2000</sub>	N-[carbonyl-methoxy(polyethylene glycol)-2000]-1,2-distearoyl-sn-glycero-3-phosphoethanolamine, sodium salt
Egg-PC	L- $\alpha$ -phosphatidylcholine
SPC	soybean phosphatidylcholine

The most important factors that influence magneto-liposomes contrast agent efficiency are shown as following:

1. The permeability of a lipid bilayer [40,41], which is determined by the phospholipid chain length, the degree of saturation and the cholesterol content;
2. Transverse relaxivity, which is a function of the water exchange rate and is proportional to the cholesterol content;
3. Even though cholesterol reduces the fluidity of a membrane, relaxivity  $r_2$  values are important for the stability in vivo;
4. Polyethylene glycol (PEG) molecules are responsible for a fixed aqueous layer thickness near liposomes, thus assisting water diffusion through the bilayer and maintaining a high hydration number. Therefore, besides the stealth effect, the inclusion of PEGylated phospholipids, such as DSPE-PEG<sub>2000</sub>, plays an important role in enhancing liposomal hydration states and consequently  $r_2$  values [41,42].

Small IO NPs usually have very low  $r_2$  values. For example, the reported highest  $r_2$  values for small IO NPs (4–5 nm) are in the range from 24 to 44  $\text{mM}^{-1} \text{s}^{-1}$  [43,44]. However, the following examples demonstrated how an appropriate coating can boost up their contrast capability [1]. Firstly, hydrophobic IO NPs embedded in a liposomal core was discussed. Bealle et al. [37] embedded citrate-coated IO NPs within magneto-liposomes composed of DPPC/DSPC (90/10 mol%) lipids. When those hydrophilic NPs (for 7 and 9 nm-sized IO NPs,  $r_2$  values were 114 and 204  $\text{mM}^{-1} \text{s}^{-1}$ , respectively) were encapsulated in the liposomal core, the  $r_2$  value increased to 138 and 267  $\text{mM}^{-1} \text{s}^{-1}$ , respectively. Moreover, Carvalho et al. [42] demonstrated a 4- to 5-fold increase in  $r_2$  value when 5 and 10 nm-sized PEGylated IO NPs ( $r_2 = 41.5$  and  $47.4 \text{ mM}^{-1} \text{ s}^{-1}$ , respectively) were encapsulated in the core of Egg PC/cholesterol/DSPE-PEG liposomes (198 and 210  $\text{mM}^{-1} \text{ s}^{-1}$ , respectively). Similarly, Skouras et al. [32] showed a high  $r_2$  value (154  $\text{mM}^{-1} \text{ s}^{-1}$ ) for DSPC/DSPE-PEG (96/4 mol%) formulation containing hydrophilic IO NPs, compared to that of plain IO NPs (76  $\text{mM}^{-1} \text{ s}^{-1}$ ).

Secondly, magneto-liposomes containing IO NPs in a bilayer have been investigated. In the work of Martínez-González et al. [39] saturated DOPC formulation had a significantly higher  $r_2$  value (630  $\text{mM}^{-1} \text{ s}^{-1}$ ) than unsaturated DMPC magneto-liposomes (340  $\text{mM}^{-1} \text{ s}^{-1}$ ), both containing oleic acid-coated IO NPs in a bilayer. These results indicated that a more fluid coating facilitates water exchange rates and thus increases  $r_2$  values. Furthermore, the same study reported the highest  $r_2$  value for DOPC-PS formulation containing oleic acid-coated IO NPs in the bilayer (PS = phosphatidylserine,  $r_2 = 995 \text{ mM}^{-1} \text{ s}^{-1}$ , while DOPC alone had an  $r_2$  value of 630  $\text{mM}^{-1} \text{ s}^{-1}$ ) [39]. PS lipid might contribute to a negatively charged surface, thus forming a more hydrated surface [45]; however, zeta potential measurements were not performed to confirm this claim.

Thirdly, cholesterol is known to increase liposome stability for in vitro and in vivo applications. However, it also reduces the fluidity of a membrane and thus the relaxivity  $r_2$  value. For example, Carvalho et al. [31] demonstrated that relaxivity  $r_2$  values of magneto-liposomes consisting of soybean PC/cholesterol and 6 nm-sized hydrophilic IO NPs were lower than those for noncholesterol-containing formulations. Moreover, it was shown that  $r_2$  strongly decreased with increasing cholesterol content in

the liposome bilayer [31]. Furthermore, Martínez-González et al. [39] showed a similar effect, that is, DOPC/cholesterol and DMPC/cholesterol liposomes containing OA-coated IO NPs exhibited lower  $r_2$  values (281 and 230  $\text{mM}^{-1} \text{s}^{-1}$ , respectively) than noncholesterol DOPC and DMPC formulations (630 and 340  $\text{mM}^{-1} \text{s}^{-1}$ , respectively).

Importantly, in all reports, all types of magneto-liposomes with higher  $r_2$  values demonstrated superior MRI capabilities, compared to free hydrophilic IO NPs. The chemical characteristic of any liposomal surface facilitates the adsorption of a water layer around the liposome and avoids the free diffusion of these molecules towards the magnetic core, resulting in high relaxivity of liposomal formulations [39]. More fluid coatings, such as unsaturated DOPC, are favourable to enhance the transverse relaxivity. PEGylation of magneto-liposomes ensures longer circulation time (stealth effect) and thus higher accumulation in tumour tissues. Additionally, it plays an important role in enhancing liposomal hydration states and consequently  $r_2$  values; therefore, it is essential to be included in the liposomal composition. Even though cholesterol reduces  $r_2$ , its addition is beneficial to maintain the liposomal stability in vivo. In our opinion, for theranostic purposes, embedding NPs in a bilayer instead of in a liposomal core is beneficial, because the core can be filled with other active components, such as chemotherapeutic drugs [38].

## 5. Biomimetic Nanostructures

Liposomes have been assumed to be one of the safest drug delivery systems developed so far. However, they are built from synthetic phospholipids. Most of synthetic NPs are recognized and eliminated as a foreign substance by the immune system. PEGylation (coating with polyethylene glycol-based molecules) of NPs is often used in liposomes and other NPs to increase circulation time and decrease elimination rates by a reticuloendothelial system. Despite the widespread use of PEG in food and drugs, people have started to show the immune response by developing the anti-PEG antibodies, which can lead to faster elimination of PEG-coated NPs [46]. Additionally, all of clinically approved IO-based MRI contrast agents have dextran-based coatings, which can cause immune responses according to the Gell–Coombs system that involves III dextran-reactive antibody reaction with the formation of immune complexes and complement activation [4]. Thus, in clinics, several preventive strategies have been applied to reduce the incidence of these reactions, such as very slow administration (>15 min), preadministration of aspirin to prevent hemodynamic reactions or low-molecular-weight dextran to block the circulation of antidextran antibodies [4]. Therefore, seeking a safer and more effective approach is urgently demanded. To achieve this, the use of the body's own cells as contrast agent carriers was proposed. Among different circulatory cells (monocyte, erythrocyte, macrophage, lymphocyte, neutrophil, platelets, leukocyte, dendritic cells, stem cells and extracellular vesicles), erythrocytes or red blood cells (RBCs) are most abundant and thus can be isolated in sufficiently large quantities to decrease the complexity and cost of treatments compared to other cell-based vaccines [47]. Therefore, state-of-the-art reports on the use of red blood cell membranes (RBCMs) as the IO NPs carriers are presented.

Up to now, only three articles (all from the same group) can be found about the encapsulation of IO NPs into RBCMs. Commercially available IO NPs (dextran- or carbodextran-coated) were encapsulated in RBCMs [48], and their biodistribution study on RBCM-coated IO NPs showed longer circulation time than PEG-coated IO NPs and lower accumulation in liver and spleen, two major organs of reticuloendothelial system (RES) [49]. A report in 2018 showed that Resovist (carbodextran-coated IO NPs) encapsulated in RBCMs can be visualized with MRI in vivo [50]. Additionally, magnetic nanoclusters coated with RBCMs showed darker tumor areas and longer-lasting contrast signals compared to magnetic nanoclusters alone, which was visualized with MRI in vivo [51]. Importantly, because the preparation of RBCMs involves the use of biological materials, strict handling protocols and rigorous blood group matching are required to maximize compatibility and avoid the risk of immunogenicity and contamination. Despite these challenges, the use of biomimetic nanosystems is a unique and exciting strategy for targeting tumor, and it is also a new paradigm of

thinking. In our opinion, a comparative study of artificially prepared cell membranes (liposomes) and naturally occurring ones (RBCMs) as carriers for magnetic NPs is required. Stability and MRI contrast efficacy should be evaluated *ex vitro*, *in vitro* and *in vivo* to obtain the answer to whether biomimetic nanostructures have better safety profile and efficacy than artificially made but clinically well-established liposomes.

## 6. Conclusions

In this review, the factors that influence the  $r_2$  values were systematically presented. In the first part, it was shown that the saturation magnetization of NPs has a crucial role in enhancing  $r_2$  values, which can be done either by increasing the particle size or via clustering. However, we are limited by the superparamagnetic size limit, above which NPs become ferromagnetic that limits their use for medical applications. In the second part, the importance of coating optimization was emphasized, and the requirements for an optimal NPs coating were listed. Magneto-liposomes were presented as an example of such optimal nanostructures. It was clearly shown that the selection of the lipid composition strongly influences the relaxivity values. Finally, a transition from synthetic towards biomimetic nanostructures to ensure inherent biocompatibility and safety is seen as a future direction in the development of contrast agents for MRI.

**Funding:** This study was supported by the Slovenian Research Agency ARRS (project numbers: Z2-9218 and P2-0084).

**Conflicts of Interest:** The author declares no conflicts of interest.

## References

1. Zhang, W.; Liu, L.; Chen, H.; Hu, K.; Delahunty, I.; Gao, S.; Xie, J. Surface impact on nanoparticle-based magnetic resonance imaging contrast agents. *Theranostics* **2018**, *8*, 2521–2548. [[CrossRef](#)]
2. Boros, E.; Gale, E.M.; Caravan, P. MR imaging probes: Design and applications. *Dalt. Trans.* **2015**, *44*, 4804. [[CrossRef](#)]
3. Wang, Y.-X.J. Superparamagnetic iron oxide based MRI contrast agents: Current status of clinical application. *Quant. Imaging Med. Surg.* **2011**, *1*, 35–40.
4. Daldrup-Link, H.E. Ten things you might not know about iron oxide nanoparticles. *Radiology* **2017**, *284*, 616–629. [[CrossRef](#)]
5. Daldrup-Link, H.E.; Rydland, J.; Helbich, T.H.; Bjørnerud, A.; Turetschek, K.; Kvistad, K.A.; Kaindl, E.; Link, T.M.; Staudacher, K.; Shames, D.; et al. Quantification of Breast Tumor Microvascular Permeability with Feruglose-enhanced MR Imaging: Initial Phase II Multicenter Trial. *Radiology* **2003**, *229*, 885–892. [[CrossRef](#)]
6. Estelrich, J.; Sanchez-Martin, M.J.; Busquets, M.A. Nanoparticles in magnetic resonance imaging: From simple to dual contrast agents. *Int. J. Nanomed.* **2015**, *10*, 1727–1741.
7. Jin, R.; Lin, B.; Li, D.; Ai, H. Superparamagnetic iron oxide nanoparticles for MR imaging and therapy: Design considerations and clinical applications. *Curr. Opin. Pharmacol.* **2014**, *18*, 18–27. [[CrossRef](#)]
8. Zhou, Z.; Yang, L.; Gao, J.; Chen, X. Structure–Relaxivity Relationships of Magnetic Nanoparticles for Magnetic Resonance Imaging. *Adv. Mater.* **2019**, *31*, 1804567. [[CrossRef](#)]
9. Lin, Y.; Wang, S.; Zhang, Y.; Gao, J.; Hong, L.; Wang, X.; Wu, W.; Jiang, X. Ultra-high relaxivity iron oxide nanoparticles confined in polymer nanospheres for tumor MR imaging. *J. Mater. Chem. B* **2015**, *3*, 5702–5710. [[CrossRef](#)]
10. Tong, S.; Hou, S.; Zheng, Z.; Zhou, J.; Bao, G. Coating optimization of superparamagnetic iron oxide nanoparticles for high T2 relaxivity. *Nano Lett.* **2010**, *10*, 4607–4613. [[CrossRef](#)]
11. Frey, N.A.; Sun, S. Magnetic Nanoparticle for Information Storage Applications. In *Inorganic Nanoparticles: Synthesis, Applications, and Perspectives*; CRC Press: Boca Raton, FL, USA, 2011; pp. 33–68.
12. Thanh, N.T.K. *Magnetic Nanoparticles: From Fabrication to Clinical Applications*; CRC Press: Boca Raton, FL, USA, 2012.
13. Şimşek, T.; Özcan, Ş. Effective magnetic anisotropy enhancement of FePt nanocrystals through shape control. *J. Magn. Magn. Mater.* **2014**, *351*, 47–51. [[CrossRef](#)]

14. Koksharov, Y.A. Magnetism of Nanoparticles: Effects of Size, Shape, and Interactions. In *Magnetic Nanoparticles*; Wiley-VCH Verlag: Weinheim, Germany, 2009; pp. 197–254. ISBN 9783527627561.
15. Issa, B.; Obaidat, I.M.; Albiss, B.A.; Haik, Y. Magnetic nanoparticles: Surface effects and properties related to biomedicine applications. *Int. J. Mol. Sci.* **2013**, *14*, 21266–21305. [[CrossRef](#)]
16. Bødker, F.; Mørup, S.; Linderoth, S. Surface effects in metallic iron nanoparticles. *Phys. Rev. Lett.* **1994**, *72*, 282–285. [[CrossRef](#)]
17. Wu, X.W.; Liu, C.; Li, L.; Jones, P.; Chantrell, R.W.; Weller, D. Nonmagnetic shell in surfactant-coated FePt nanoparticles. *J. Apply. Phys.* **2004**, *95*, 6810–6812. [[CrossRef](#)]
18. Tanaka, Y.; Saita, S.; Maenosono, S. Influence of surface ligands on saturation magnetization of FePt nanoparticles. *Appl. Phys. Lett.* **2008**, *92*, 47–50. [[CrossRef](#)]
19. Na, H.B.; Song, I.C.; Hyeon, T. Inorganic nanoparticles for MRI contrast agents. *Adv. Mater.* **2009**, *21*, 2133–2148. [[CrossRef](#)]
20. Shin, T.; Choi, Y.; Kim, S.; Cheon, J. Recent advances in magnetic nanoparticle-based multi-modal imaging. *Chem. Soc. Rev.* **2015**, *44*, 4501–4516. [[CrossRef](#)]
21. Balasubramaniam, S.; Kayandan, S.; Lin, Y.-N.; Kelly, D.F.; House, M.J.; Woodward, R.C.; St Pierre, T.G.; Riffle, J.S.; Davis, R.M. Toward design of magnetic nanoparticle clusters stabilized by biocompatible diblock copolymers for T<sub>2</sub>-weighted MRI contrast. *Langmuir* **2014**, *30*, 1580–1587. [[CrossRef](#)]
22. Lartigue, L.; Hugounenq, P.; Alloyeau, D.; Clarke, S.P.; Lévy, M.; Bacri, J.C.; Bazzi, R.; Brougham, D.F.; Wilhelm, C.; Gazeau, F. Cooperative organization in iron oxide multi-core nanoparticles potentiates their efficiency as heating mediators and MRI contrast agents. *ACS Nano* **2012**, *6*, 10935–10949. [[CrossRef](#)]
23. Kostevšek, N.; Šturm, S.; Serša, I.; Sepe, A.; Bloemen, M.; Verbiest, T.; Kobe, S.; Žužek Rožman, K. “Single-” and “multi-core” FePt nanoparticles: From controlled synthesis via zwitterionic and silica bio-functionalization to MRI applications. *J. Nanoparticle Res.* **2015**, *17*, 464. [[CrossRef](#)]
24. Caravan, P.; Farrar, C.T.; Frullano, L.; Uppal, R. Influence of molecular parameters and increasing magnetic field strength on relaxivity of gadolinium- and manganese-based T<sub>1</sub> contrast agents. *Contrast Media Mol. Imaging* **2009**, *4*, 89–100. [[CrossRef](#)]
25. Kostevšek, N.; Abramovič, I.; Hudoklin, S.; Kreft, M.E.; Serša, I.; Sepe, A.; Vidmar, J.; Šturm, S.; Spreitzer, M.; Ščančar, J.; et al. Hybrid FePt/SiO<sub>2</sub>/Au nanoparticles as a theranostic tool: In vitro photo-thermal treatment and MRI imaging. *Nanoscale* **2018**, *10*, 1308–1321. [[CrossRef](#)]
26. Zeng, J.; Jing, L.; Hou, Y.; Jiao, M.; Qiao, R.; Jia, Q.; Liu, C.; Fang, F.; Lei, H.; Gao, M. Anchoring group effects of surface ligands on magnetic properties of Fe<sub>3</sub>O<sub>4</sub> nanoparticles: Towards high performance MRI contrast agents. *Adv. Mater.* **2014**, *26*, 2694–2698. [[CrossRef](#)]
27. Damodaran, K.V.; Merz, K.M.; Gaber, B.P. Structure and Dynamics of the Dilauroylphosphatidylethanolamine Lipid Bilayer. *Biochemistry* **1992**, *31*, 7656–7664. [[CrossRef](#)]
28. Dumas, S.; Jacques, V.; Sun, W.-C.; Troughton, J.S.; Welch, J.T.; Chasse, J.M.; Schmitt-Willich, H.; Caravan, P. High relaxivity magnetic resonance imaging contrast agents. Part 1. Impact of single donor atom substitution on relaxivity of serum albumin-bound gadolinium complexes. *Invest. Radiol.* **2010**, *45*, 600–612. [[CrossRef](#)]
29. Kneidl, B.; Peller, M.; Winter, G.; Lindner, L.H.; Hossann, M. Thermosensitive liposomal drug delivery systems: State of the art review. *Int. J. Nanomed.* **2014**, *9*, 4387–4398.
30. Shen, S.; Huang, D.; Cao, J.; Chen, Y.; Zhang, X.; Guo, S.; Ma, W.; Qi, X.; Ge, Y.; Wu, L. Magnetic liposomes for light-sensitive drug delivery and combined photothermal–chemotherapy of tumors. *J. Mater. Chem. B* **2019**, *7*, 1096–1106. [[CrossRef](#)]
31. Carvalho, A.; Goncalves, M.C.; Martins, M.B.F.; Meixedo, D.; Feio, G. Relaxivities of magnetoliposomes: The effect of cholesterol. *Magn. Reson. Imaging* **2013**, *31*, 610–612. [[CrossRef](#)]
32. Skouras, A.; Mourtas, S.; Markoutsas, E.; De Goltstein, M.-C.; Wallon, C.; Catoen, S.; Antimisariis, S.G. Magnetoliposomes with high USPIO entrapping efficiency, stability and magnetic properties. *Nanomed. Nanotechnol. Biol. Med.* **2011**, *7*, 572–579. [[CrossRef](#)]
33. Garnier, B.; Tan, S.; Miraux, S.; Bled, E.; Brisson, A.R. Optimized synthesis of 100 nm diameter magnetoliposomes with high content of maghemite particles and high MRI effect. *Contrast Media Mol. Imaging* **2012**, *7*, 231–239. [[CrossRef](#)]
34. Marie, H.; Lemaire, L.; Franconi, F.; Lajnef, S.; Frapart, Y.-M.; Nicolas, V.; Frebourg, G.; Trichet, M.; Menager, C.; Lesieur, S. Superparamagnetic Liposomes for MRI Monitoring and External Magnetic Field-Induced Selective Targeting of Malignant Brain Tumors. *Adv. Funct. Mater.* **2015**, *25*, 1258–1269. [[CrossRef](#)]

35. Faria, M.R.; Cruz, M.M.; Gonçalves, M.C.; Carvalho, A.; Feio, G.; Martins, M.B.F. Synthesis and characterization of magnetoliposomes for MRI contrast enhancement. *Int. J. Pharm.* **2013**, *446*, 183–190. [[CrossRef](#)] [[PubMed](#)]
36. Martina, M.S.; Fortin, J.P.; Ménager, C.; Clément, O.; Barratt, G.; Grabielle-Madellmont, C.; Gazeau, F.; Cabuil, V.; Lesieur, S. Generation of superparamagnetic liposomes revealed as highly efficient MRI contrast agents for in vivo imaging. *J. Am. Chem. Soc.* **2005**, *127*, 10676–10685. [[CrossRef](#)]
37. Béalle, G.; Di Corato, R.; Kolosnjaj-Tabi, J.; Dupuis, V.; Clément, O.; Gazeau, F.; Wilhelm, C.; Ménager, C. Ultra magnetic liposomes for MR imaging, targeting, and hyperthermia. *Langmuir* **2012**, *28*, 11834–11842. [[CrossRef](#)]
38. Guo, Y.; Zhang, Y.; Ma, J.; Li, Q.; Li, Y.; Zhou, X.; Zhao, D.; Song, H.; Chen, Q.; Zhu, X. Light/magnetic hyperthermia triggered drug released from multi-functional thermo-sensitive magnetoliposomes for precise cancer synergetic theranostics. *J. Control. Release* **2018**, *272*, 145–158. [[CrossRef](#)]
39. Martínez-González, R.; Estelrich, J.; Busquets, M.A. Liposomes Loaded with Hydrophobic Iron Oxide Nanoparticles: Suitable T<sub>2</sub> Contrast Agents for MRI. *Int. J. Mol. Sci.* **2016**, *17*, 1209. [[CrossRef](#)]
40. Ferrauto, G.; Delli Castelli, D.; Di Gregorio, E.; Terreno, E.; Aime, S. LipoCEST and cellCEST imaging agents: Opportunities and challenges. *WIREs Nanomed. Nanobiotechnol.* **2016**, *8*, 602–618. [[CrossRef](#)]
41. Carvalho, A.; Gonçalves, M.C.; Corvo, M.L.; Martins, M.B.F. Development of New Contrast Agents for Imaging Function and Metabolism by Magnetic Resonance Imaging. *Magn. Reson. Insights* **2017**, *10*. [[CrossRef](#)]
42. Carvalho, A.; Martins, M.B.F.; Corvo, M.L.; Feio, G. Enhanced contrast efficiency in MRI by PEGylated magnetoliposomes loaded with PEGylated SPION: Effect of SPION coating and micro-environment. *Mater. Sci. Eng. C* **2014**, *43*, 521–526. [[CrossRef](#)]
43. Li, J.; Shi, X.; Shen, M. Hydrothermal Synthesis and Functionalization of Iron Oxide Nanoparticles for MR Imaging Applications. *Part. Part. Syst. Charact.* **2014**, *31*, 1223–1237. [[CrossRef](#)]
44. Li, Z.; Yi, P.W.; Sun, Q.; Lei, H.; Li Zhao, H.; Zhu, Z.H.; Smith, S.C.; Lan, M.B.; Lu, G.Q. Ultrasmall water-soluble and biocompatible magnetic iron oxide nanoparticles as positive and negative dual contrast agents. *Adv. Funct. Mater.* **2012**, *22*, 2387–2393. [[CrossRef](#)]
45. Scheu, R.; Rankin, B.M.; Chen, Y.; Jena, K.C.; Ben-Amotz, D.; Roke, S. Charge asymmetry at aqueous hydrophobic interfaces and hydration shells. *Angew. Chem. Int. Ed.* **2014**, *126*, 9714–9717. [[CrossRef](#)]
46. Li, R.; He, Y.; Zhang, S.; Qin, J.; Wang, J. Cell membrane-based nanoparticles: A new biomimetic platform for tumor diagnosis and treatment. *Acta Pharm. Sin. B* **2018**, *8*, 14–22. [[CrossRef](#)]
47. Phua, K.K.L.; Boczkowski, D.; Dannull, J.; Pruitt, S.; Leong, K.W.; Nair, S.K. Whole Blood Cells Loaded with Messenger RNA as an Anti-Tumor Vaccine. *Adv. Healthc. Mater.* **2014**, *3*, 837–842. [[CrossRef](#)]
48. Antonelli, A.; Sfara, C.; Manuali, E.; Bruce, I.J.; Magnani, M. Encapsulation of superparamagnetic nanoparticles into red blood cells as new carriers of MRI contrast agents. *Nanomedicine* **2011**, *6*, 211–223. [[CrossRef](#)]
49. Rao, L.; Bu, L.L.; Xu, J.H.; Cai, B.; Yu, G.T.; Yu, X.; He, Z.; Huang, Q.; Li, A.; Guo, S.S.; et al. Red Blood Cell Membrane as a Biomimetic Nanocoating for Prolonged Circulation Time and Reduced Accelerated Blood Clearance. *Small* **2015**, *11*, 6225–6236. [[CrossRef](#)]
50. Antonelli, A.; Pacifico, S.; Sfara, C.; Tamma, M.; Magnani, M. Ferucarbotran-loaded red blood cells as long circulating MRI contrast agents: First in vivo results in mice. *Nanomedicine* **2018**, *13*, 675–687. [[CrossRef](#)]
51. Ren, X.; Zheng, R.; Fang, X.; Wang, X.; Zhang, X.; Yang, W.; Sha, X. Red blood cell membrane camouflaged magnetic nanoclusters for imaging-guided photothermal therapy. *Biomaterials* **2016**, *92*, 13–24. [[CrossRef](#)]

